Nanoscale

Revealing Principal Attributes of Protein Adsorption on Block Copolymer Surfaces with Direct Experimental Evidence at the Single Protein Level

Journal:	*Nanoscale*
Manuscript ID	NR-ART-02-2018-001371.R1
Article Type:	Paper
Date Submitted by the Author:	30-Mar-2018

Complete List of Authors:	Xie, Tian; Georgetown University, Department of Chemistry Chattoraj, Joyjit; Georgetown University, Physics; Nanyang Technological University, Physics and Applied Physics Mulcahey, Patrick; Georgetown University, Department of Chemistry Kelleher, Noah; Georgetown University, Department of Chemistry Del Gado, Emanuela; Georgetown University, Physics; ETH Zurich, Civil, Environmental and Geomatic Engineering Hahm, Jong-in; Georgetown University, Department of Chemistry

Revealing Principal Attributes of Protein Adsorption on Block Copolymer Surfaces with Direct Experimental Evidence at the Single Protein Level

*Tian Xie[†], Joyjit Chattoraj[‡,§], Patrick J. Mulcahey[†], Noah P. Kelleher[†], Emanuela Del Gado[‡], and Jong-in Hahm[†,]**

[†]Department of Chemistry and [‡] Department of Physics, Georgetown University, 37th & O Sts. NW., Washington, DC 20057, USA

[§] Present Address: Division of Physics and Applied Physics, School of Physical and Mathematical Sciences, Nanyang Technological University, 21 Nanyang Link, Singapore 637371

**Address Correspondence to jh583@georgetown.edu*

ABSTRACT

Understanding protein adsorption onto polymer surfaces is of great importance in designing biomaterials, improving bioanalytical devices, and controlling biofouling, to name a few examples. Although steady research efforts have been advancing this field, our knowledge of this ubiquitous and complex phenomenon is still limited. In this study, we elucidate competitive protein adsorption behaviors sequentially occurring onto nanoscale block copolymer (BCP) surfaces via combined experimental and computer simulation approaches. The model systems chosen for our investigation are immunoglobulin G and fibrinogen introduced in different orders to the self-assembled nanodomains of poly(styrene)-*block*-poly(methylmethacrylate). We unambiguously reveal the adsorption, desorption, and replacement events of the same protein molecules via single protein tracking with atomic force microscopy. We then ascertain adsorption-related behaviors such as lateral mobility and self-association of proteins. We provide much-needed, direct experimental proof of sequential adsorption events at the biomolecule level, which was virtually nonexistent before. We determine key protein adsorption pathways and dominant tendencies of sequential protein adsorption. We also reveal preadsorbed surface-associated behaviors in sequential adsorption, distinct from situations involving initially empty surfaces. We perform Monte-Carlo simulations to further substantiate our experimental outcomes. Our endeavors in this study may facilitate a well-guided mechanistic understanding of protein-polymer interactions by providing definite experimental evidence of competitive, sequential adsorption on the nanoscale. Increasingly, biomaterial and biomedical applications rely on systems of multicomponent proteins and chemically intricate, nanoscale polymer surfaces. Hence, our findings can also be beneficial to the development of next-generation nanobiomaterials and nanobiosensors exploiting self-assembled BCP nanodomain surfaces.

Keywords: Block Copolymer, Protein-Surface Interaction, Protein-Polymer Interaction, Competitive Protein Adsorption, Sequential Protein Adsorption, Single Protein Tracking, Protein Adsorption Mechanism

INTRODUCTION

The ubiquitous phenomenon of protein adsorption to solid surfaces is of paramount importance, affecting a wide range of fields such as biomaterials, biosensors, implants, tissue engineering, and food packaging.[1-4] The processes of protein adsorption occurring firstly to the surfaces of *in vivo* biodevices and biomaterials are known to be central in the integration of implanted devices and scaffolds by affecting subsequent cell growths or cellular response behaviors.[2,4-6] For solid state biosensors and bioprobes, the surface density, configuration, and functionality of adsorbed proteins can significantly influence their quantitative measurement outcomes.[7-10] Therefore, understanding and controlling protein adsorption to solid interfaces will be critical to providing not only fundamentally valuable knowledge but also technologically important design principles.

In this regard, we have previously studied protein adsorption behaviors of single component proteins on block copolymers (BCPs).[11-13] Both experimentally and theoretically, it is well-established that chemically distinctive polymeric blocks in BCPs can be thermodynamically controlled to produce periodically arranged, nanoscale patterns of controlled sizes and shapes via self-assembly.[14-19] BCPs have shown high biomedical relevance, with increasing utility in biologically geared applications.[20,21] For example, proteins and cells are known to respond to the periodic surface features of varying chemistries and sizes of BCPs.[11,22-25] In addition, BCPs have been demonstrated to be convenient and well-controlled templates for protein adsorption.[18,22-24,26-29] Therefore, the use of BCPs in biomaterials, biosensors, and biodevices is likely to expand further, and the understanding of their roles in interfacing proteins and cells will become ever more important.

Atomic force microscopy (AFM) is the detection method of choice for examining discrete proteins bound to the BCP surfaces.[18] Various techniques can be employed for investigating protein adsorption in general. They include infrared spectroscopy,[30-32] x-ray photoelectron spectroscopy,[33-35] ellipsometry,[36-38] total internal reflection and related fluorescence techniques,[39-42] surface plasmon resonance,[43-45] quartz crystal microbalance,[31,36] and optical waveguide lightmode spectroscopy.[46-48] However, AFM offers sufficiently high spatial resolution for simultaneously resolving the nanometer-

sized individual proteins and the underlying polymeric BCP nanodomains[18,23,24] and can be used to measure biomolecular adhesion forces onto different surfaces via single molecule force measurements.[18,23,24,49,50] AFM also has the advantage of circumventing the need for crystallization, labelling, conductive metal coating, or high vacuum/low temperature operation of protein samples.[51-53]

Real-life biomedical applications of BCPs are expected to involve multiple protein components, rather than single protein constituents. Yet, even less is understood about multi-component protein adsorption processes, warranting further experimental and computational investigations. For examining competitive adsorption, the direct visualization capability of AFM to be able to discern different protein species based on their sizes and shapes may be exploited. It can be used to directly track particular proteins of interest on the same surface areas and record changes in their adsorption behaviors between different treatments. Such an approach may offer definitive experimental evidence for many postulations made in protein adsorption mechanisms[1,2] that are, at present, often inferred from ensemble-averaged adsorption properties[5,38,40,54-61] due to the lack of direct experimental proof at the single biomolecule level.

Herein, we ascertain competitive protein adsorption behaviors that occur sequentially onto the nanoscale BCP surface of poly(styrene)-*block*-poly(methylmethacrylate) (PS-*b*-PMMA) by using IgG and Fg as model protein components. The same sets of individual IgG and Fg as well as PS-*b*-PMMA nanodomains are faithfully tracked and unambiguously resolved at the individual protein level by acquiring a time-lapse series of high resolution AFM frames from the same surface locations. We record the adsorption/desorption/displacement events of each protein on PS-*b*-PMMA. We also provide experimental proof for protein behaviors such as lateral mobility on the surface, tendency for proximal/distal adsorption, occurrence frequency for different adsorption pathways, and directionality in protein exchange. In addition, we elucidate preadsorbed surface-associated behaviors in which the subsequent stage protein adsorption is influenced by the amounts of prebound proteins on the surface, rather than by the bulk concentration of the newly adsorbing proteins. By means of Monte-Carlo (MC) simulations of a simple model, we further corroborate with the experimental outcomes of preadsorbed

surface-dependence and rationalize main adsorption events in terms of the model parameters. Our findings in this study will be important for building the much-needed knowledge base on competitive protein adsorption. By providing definitive experimental evidence on sequential protein adsorption onto nanoscale surfaces, our results may also open up a better mechanistic understanding of protein adsorption processes and subsequently aid in the development of new BCP-based biomaterials and biosensors.

METHODS

Experimental Method. The periodic nanodomain surfaces of PS and PMMA blocks were prepared from PS-*b*-PMMA diblock copolymer (71% PS by weight) with an average molecular weight of 71.4 kDa and a polydispersity of 1.06 which was obtained from Polymer Source Inc. (Montreal, Canada). Silicon wafers were obtained from Silicon Quest, Inc.(San Jose, CA) and prepared into 1 by 1 cm^2 pieces. They were cleaned with ethanol, acetone, and toluene and spun dry before being coated with the BCP. An ultrathin film of the BCP was produced by spincasting a 2 % (w/v) solution of the specified BCP in toluene onto the pre-cleaned Si surface at 3500 rpm for 1 min. The BCP substrate was subsequently annealed in an Ar atmosphere at 240 °C for 8 h with a transient ramp-up rate of 5 °C/min and a cooling rate of 2 °C/min. This thermal annealing process induced phase separation of the PS and PMMA chains in the BCP, yielding periodically alternating and chemically varying nanodomains known as half-cylinders and exposing repeating stripes of PS and PMMA blocks at the air/polymer interface with repeat units of 45 nm (PS to PS distance).[11]

Whole molecule bovine IgG and human plasma Fg were received from VWR Scientific Inc. (West Chester, PA) in a lyophilized form and reconstituted in PBS buffer (10 mM mixture of Na_2HPO_4 and NaH_2PO_4, 140 mM NaCl, 3 mM KCl, pH 7.4). The reconstituted protein solutions were then diluted to various concentrations ranging from 0.01 μg/mL to 25 μg/mL in PBS. A 10 μL volume of IgG or Fg solution with a desired concentration was deposited on the polymeric substrate for a period of 20 s to 15 min. The sample surfaces were then carefully rinsed with PBS multiple times and gently dried under a

stream of N_2 prior to AFM imaging. For multistage protein deposition, the protein solution of interest was subsequently applied on the BCP containing preadsorbed protein species from the prior deposition step. Between each solution treatment, the sample was rinsed with an ample amount of PBS and dried with N_2. A MultiMode 8 AFM interfaced with a Nanoscope V controller (Bruker Corp., Santa Barbara, CA) was used to collect the topography and phase images from the same BCP surface areas. The same set of IgG and Fg proteins on the same locations of PS-*b*-PMMA were tracked by performing high resolution AFM imaging between different solution treatments. Faithful protein tracking to record sequentially occurring adsorption events was possible by unambiguously resolving both the individual IgG and Fg protein molecules as well as the distinct nanoscopic details of underlying polymeric nanodomains after each deposition step. AFM was operated in a soft tapping mode at a scan speed of 1 Hz or lower, using Si tips with a typical resonant frequency of 60-70 kHz and a spring constant of ~1 N/m.

Simulational Method. MC simulations were carried out to further substantiate the experimental outcomes of preadsorbed surface-dependence on subsequent stage protein adsorption. Proteins were simply considered to be circular disks which interact with one another via steric repulsion as defined below,

$$U(r_{ij}) = \varepsilon \left(\frac{\sigma}{r_{ij}}\right)^{12}$$

r_{ij} is their center-to-center distance, σ is the arithmetic mean of the diameters σ_i and σ_j of proteins i and j, respectively, and ε is the interaction strength that we used as energy unit in the simulations. To facilitate the numerical implementation with the use of periodic boundary conditions, the potential function was truncated at $r_c = 2.5\,\sigma_{ij}$ where the interaction energy is already negligible with respect to ε and a small constant term was added to $U(r_{ij})$ to ensure that it smoothly reaches the zero-value at r_c.[62] We used a 2D simulation box to mimic the polymer surface. Protein interactions with the polymer surface were subsequently modeled by reflecting that, proportional to their size, proteins can adsorb on the polymer surface with an energy gain of ΔE as shown below.[63]

$$\Delta E\ (\sigma_i\ ) = \ -\varepsilon\ \left(\frac{\sigma_i}{\sigma}\right)^2$$

A MC step corresponds to the attempt to adsorb and desorb a protein chosen at random to and from the substrate. The total protein-protein interaction energy for N numbers of proteins on the substrate U_N can be expressed as the following.

$$U_N = \sum_{i=1}^{N-1} \sum_{j=i+1}^{N} U(r_{ij})$$

Using a Metropolis MC algorithm,[62] the acceptance probability for a new protein to be adsorbed or desorbed can be written as below.

$$W(N \to N+1) = \ W(N+1 \to N) = \ \min[1, e^{-\frac{(\Delta U + \Delta E)}{k_B T}}]$$

$$\Delta U = \ U_{N+1} - \ U_N$$

k_B is the Boltzmann constant and T is the temperature. By setting ε as the unit energy, we controlled the parameter of $\frac{k_B T}{\varepsilon}$ that quantifies the strength of the protein-protein interactions and that of the surface-protein interactions with respect to room temperature. All simulation data in this paper refer to $\frac{k_B T}{\varepsilon} \ll 1$, corresponding to a strong affinity between the surface and the proteins, that were obtained for a squared simulation box of a linear size $L = 70\sigma$ where σ is the unit length. To mimic the interplay between the two different protein types in the experiments, we considered disks of two different diameters, 0.6σ and 1.2σ, respectively. The diameters of 0.6σ and 1.2σ chosen in this study are consistent with the previously used size estimations for IgG and 'lying-down' Fg, respectively.[57] In each simulation, we attempted to adsorb/desorb proteins of N_{max}, which is equivalent to a given bulk concentration.

RESULTS AND DISCUSSION

Structure of Model Proteins. IgG is made up of four polypeptide chains with two identical light chains (L chains, 25 kDa each) and two identical heavy chains (H chains, 50 kDa each), forming a Y-shaped

structure with a molecular weight of 150 kDa.[64,65] The dimensions of IgG are estimated to be 14.5 nm by 8.5 nm by 4.0 nm based on X-ray crystallographic data.[64] Compared to IgG, Fg is highly elongated in its shape, exhibiting a length-to-width anisotropy of ~10:1.[23] The 340 kDa dimeric protein of Fg is composed of three interwoven polypeptide chains of Aα, Bβ and γ that are linked by coiled-coil connectors. The structure of Fg contains rod-like chains spanning two distal D domains and one centrally located E domain. Fg was first imaged by electron microscopy (EM), revealing its molecular length of ~47 nm with roughly spherical D and E domains.[66] Later, more intricate Fg structures were revealed based on crystallographic, EM, and AFM data, which additionally show split D domains and αC chains stemming from each D domain.[67-70]

These two proteins were chosen as the model systems due to their importance in basic biological research/biomedical applications, the large difference in their shape anisotropy, and the pre-existing bulk adsorption data. IgG and Fg are abundant proteins in blood and, hence, materials coated with these proteins play a central role in the fields of biosensors and implants.[53,54,57,58] Therefore, extensive literature on the bulk and macroscopic scale adsorption of IgG and Fg onto different solid surfaces exists in biomaterials, thrombosis, and hemotology.[20,37,45,53-58,61,69,71] Surface-adsorbed IgG and Fg molecules are also frequently employed in basic research and biotechnology in the form of protein arrays, solid-state biosensors, and protein patches.[8-10,71] In addition, the large shape difference between the globular IgG and the elongated Fg renders straightforward identification of the two proteins using AFM. For IgG bound on PS-*b*-PMMA, the overall shape is typically resolved by AFM as a sphere-like object of approximately 15 nm in diameter and 2.5 nm in height.[11] Fg on PS-*b*-PMMA is often seen as a boomerang-shaped object whose overall length can be approximated to be 45 nm (spanning the D-E-D domains with folded αC) with an average spherical domain height of 2.2 nm by AFM.[23]

AFM Tracking of Individual Proteins. Using these model proteins, we examined characteristic adsorption behaviors upon sequential introduction of the protein species to the BCP surface of PS-*b*-PMMA. All data reported in this study correspond to low surface coverage regimes where protein

loading on the surface was kept below a monolayer in order to clearly resolve individual proteins and BCP nanodomains of interest. AFM imaging was carried out repeatedly on the same PS-*b*-PMMA surface locations between each protein deposition stage. Any changes on the surface were faithfully recorded to reveal characteristic adsorption behaviors from the same sets of proteins before and after sequential treatments. Specific activities that the individual proteins underwent, such as adsorption, desorption, and replacement, were then identified. The schematic illustrated in Fig. 1(A) depicts the overall AFM tracking process of the same PS-*b*-PMMA area exposed to different protein species or neat buffer in a multistep process of solution deposition. The underlying PS-*b*-PMMA template used in this study exhibits fingerprint-like patterns of 45 nm in repeat spacing.[11] The fingerprint patterns expose alternating PS and PMMA nanodomains to the air/polymer interface.[11,18] In all AFM data presented in this study, the PS and PMMA nanodomains appear as darker (orange) and lighter (yellow) regions, respectively. These nanodomain patterns on the BCP surface serve as convenient markers to return to the same areas for protein tracking. AFM panels shown in Figs. 1(B) and 1(C) are a representative series of topographic and phase scans captured before and after Fg introduction to a PS-*b*-PMMA surface pretreated with IgG. The paired AFM images in Figs. 1(B) and 1(C) were acquired from the same PS-*b*-PMMA location before and after the Fg treatment. It can be seen clearly from the zoomed-in phase panels in Fig. 1(C) that the PS-*b*-PMMA surface was changed from initially containing only the short, round particles of IgG (left frames) to displaying more of the long, boomerang-shaped Fg molecules (right frames). The AFM tracking of individual proteins enabled us to directly visualize the specific sequential adsorption events that each protein underwent, of which conclusive evidence was not experimentally available before. Furthermore, such direct monitoring of individual protein behaviors allowed us to determine predominant adsorption trends and pathways in sequential protein adsorption. These findings are detailed herein.

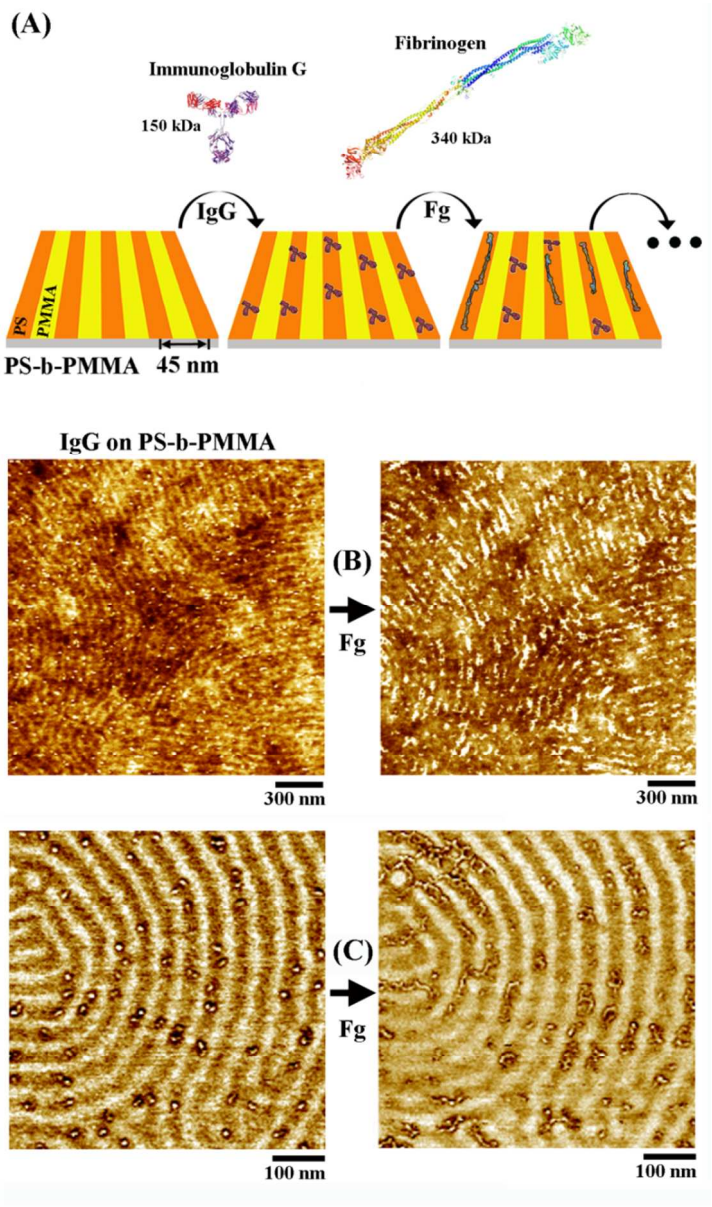

Figure 1. (A) Schematic illustrations displaying our sequential protein adsorption experiments on PS-*b*-PMMA. AFM imaging was carried out on the same BCP nanodomain regions after each treatment step involving either a protein or neat buffer solution. Individual proteins from the same surface areas were tracked to study consecutively occurring events such as protein adsorption, desorption, and replacement. **(B-C)** A representative series of AFM panels showing our typical AFM tracking data obtained from the same surface sites. The panels in (B) and (C) correspond to the BCP surface after introduction of an IgG solution to a clean PS-*b*-PMMA template (left column) and the same PS-*b*-PMMA location after exposure to a Fg solution (right column). AFM images in (B) are topographic panels and those in (C) are phase images.

Two-Stage Tracking of Individual Proteins. Sequential adsorption events on PS-*b*-PMMA were further scrutinized and analyzed to determine the exact changes associated with individual proteins. AFM data in Fig. 2(A) display typical phase frames acquired after initial IgG deposition followed by a second deposition step of Fg. Examples of tracking distinct adsorption events associated with discrete IgG molecules are provided in the high-magnification panels of Figs. 2(B) and 2(C). Specifically, Fig. 2(B) follows the different activities of four IgG molecules adsorbed initially on a PS-*b*-PMMA surface. The ensuing Fg deposition led to the replacement of two IgG molecules with three newly bound Fg molecules. Another example in Fig. 2(C) shows a different scenario in which two initially adsorbed IgG molecules remained on the surface upon Fg introduction and two new Fg molecules appeared by taking up surface sites unoccupied by IgG.

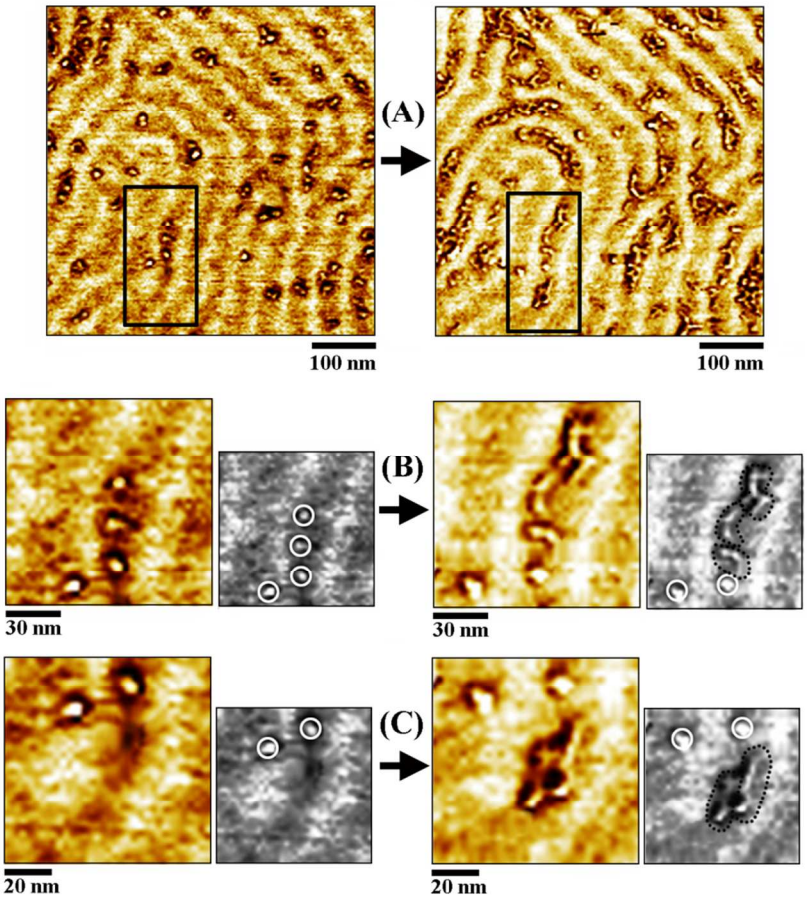

Figure 2. AFM phase images of representative data sets tracking individual proteins between different deposition steps to determine distinct adsorption events associated with each protein. **(A)** AFM panels acquired from an identical PS-*b*-PMMA location are shown side by side for direct comparison of the dynamic events occurring on the same polymeric surface area after introduction of an IgG solution (left) and subsequent exposure to a Fg solution (right). **(B and C)** Different examples of serial protein adsorption events are displayed in the higher magnification AFM panels, revealing the distinctive activities of the individual IgG molecules found inside the inserted box in (A). For clarity, the colored AFM phase data are also shown as grey scale images whose panels contain marked proteins (IgG and Fg with solid white and dashed black circles, respectively) for easy correlation of the changes between the sequential adsorption steps. In (B), the sequential adsorption event led to the displacement of two IgG molecules originally adsorbed on the surface by three Fg molecules. In (C), the two initially adsorbed IgG molecules remained on the BCP surface, whereas the two new Fg molecules took up empty surface sites void of IgG.

Five Common Adsorption Events. We carefully evaluated a large set of AFM images (over 100 frames of 2x2 μm^2 in size) obtained from the same PS-*b*-PMMA areas before and after the two-stage deposition process of IgG followed by Fg. Each type of adsorption event that the proteins engaged in was catalogued to classify main types of sequential adsorption pathways. Five different pathways were identified from the analyses, as summarized in Fig. 3. Representative AFM images in Fig. 3(A) show all five of the predominant adsorption pathways which are schematically illustrated in Fig. 3(B). The sequential adsorption process can result in cases where the initially bound protein species are left persistently adsorbed on the surface even after the introduction of a 2^{nd} protein species (i, persistent adsorption). The process can also lead to desorption of the initially adsorbed protein species, generating empty surface sites (ii, desorption with new empty sites). Alternatively, the process can lead to the replacement of initially adsorbed protein species by the 2^{nd} stage protein molecules (iii,

replacement/exchange). In addition, the sequential adsorption process can trigger the 2nd stage species to adsorb in close proximity to the initially bound proteins (iv, proximal adsorption). Finally, the process can produce adsorption of the 2nd protein species on empty surface sites away from the initially bound proteins (v, distal adsorption). The analysis criteria we used to differentiate the two cases of (iv) proximal versus (v) distal adsorption was the diameter of the 1st stage protein, and a binding event was considered as a proximal case if Fg appeared within 15 nm of surface-bound IgG in any direction. In Fig. 3(A), the different examples of these sequential adsorption pathways are marked as (i) through (v), next to each protein that underwent the specified process.

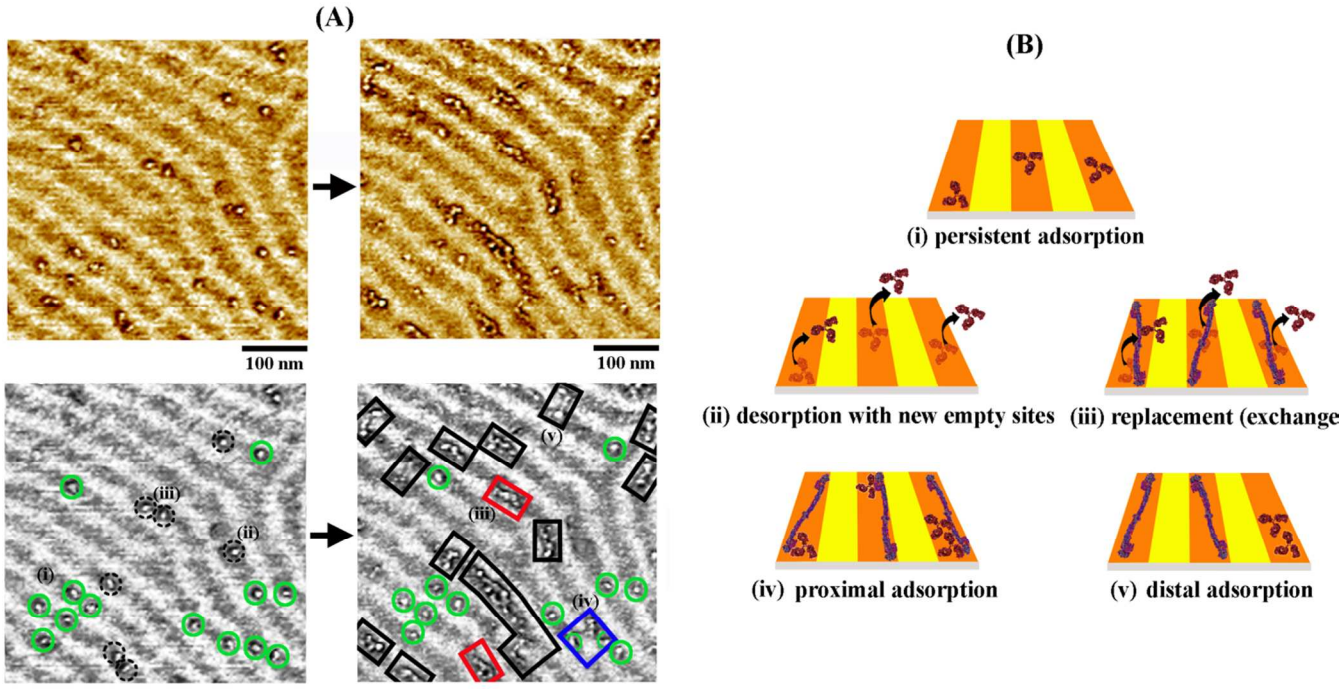

Figure 3. The five different, commonly found pathways of sequential protein adsorption are summarized. **(A)** The representative AFM phase panels contain protein adsorption evolving via the five different pathways. The grey scale AFM images are identical to the colored panels above, and the proteins are marked to clearly show the different adsorption events frequently observed in our serial protein deposition experiments. IgG molecules can remain as undisturbed on the BCP surface after the exposure to a Fg solution (i, solid green circles). IgG molecules can also desorb after the Fg

introduction, resulting in either empty surface sites (ii, black dashed circles) or sites now occupied by Fg (iii, red boxes). Additionally, Fg molecules can adsorb in close proximity to the initially bound IgG (iv, blue boxes) or at empty sites originally unoccupied by IgG (v, black boxes). For clarity, grey scale panels are provided to follow the specific adsorption pathway for each protein. **(B)** Cartoons illustrating the five common protein adsorption pathways discussed above. The dynamic process of sequential protein adsorption can lead to (i) persistent adsorption, (ii) desorption with new empty sites, (iii) replacement (exchange), (iv) proximal adsorption, and (v) distal adsorption.

Three-Stage Tracking of Individual Proteins. Next, we carried out three successive protein depositions of varying sequences for AFM tracking of individual proteins. The series of AFM panels displayed in Fig. 4 correspond to the sequential protein deposition of 0.1 μg/mL IgG for 30 s (1st stage) followed by 1 μg/mL Fg for 15 min (2nd stage) and then by 0.1 μg/mL IgG for 5 min (3rd stage) to a PS-*b*-PMMA surface, whereas the data set in Fig. 5 pertains to the solution deposition of 0.1 μg/mL IgG for 30 s (1st stage) followed by PBS for 15 min (2nd stage) and subsequently by 1 μg/mL Fg for 15 min (3rd stage). The high propensity of Fg to replace IgG, but not the reverse exchange, can be clearly seen in the IgG → Fg → IgG series in Fig. 4. The transition from the 1st → 2nd stage yielded quite a few IgG molecules replaced by Fg molecules. In contrast, the ensuing transition from the 2nd → 3rd stage caused no desorption of the Fg molecules adsorbed in the 2nd stage. This behavior was observed regardless of the specific pathways taken by the Fg molecules that led to their initial surface adsorption. The color-coded boxes in Fig. 4 mark the exact type of adsorption pathway utilized by each Fg molecule during the 2nd stage. The cases of Fg replacing IgG, proximal Fg adsorption, and distal Fg adsorption are indicated in red, blue, and black, respectively. Regardless of their initial adsorption pathways, all Fg molecules remained bound on the PS-*b*-PMMA surface, and subsequent IgG adsorption in the 3rd stage took place by landing on freely available surface sites. In the sequential treatment series of IgG → PBS

→ Fg in Fig. 5, it is evident that no desorption of the initially adsorbed IgG molecules occurred during the 2nd stage of neat buffer treatment. In contrast, further introduction of Fg solution in the 3rd stage drove the persistently adsorbed IgG molecules to detach from the surface, even leading to IgG replacement by Fg.

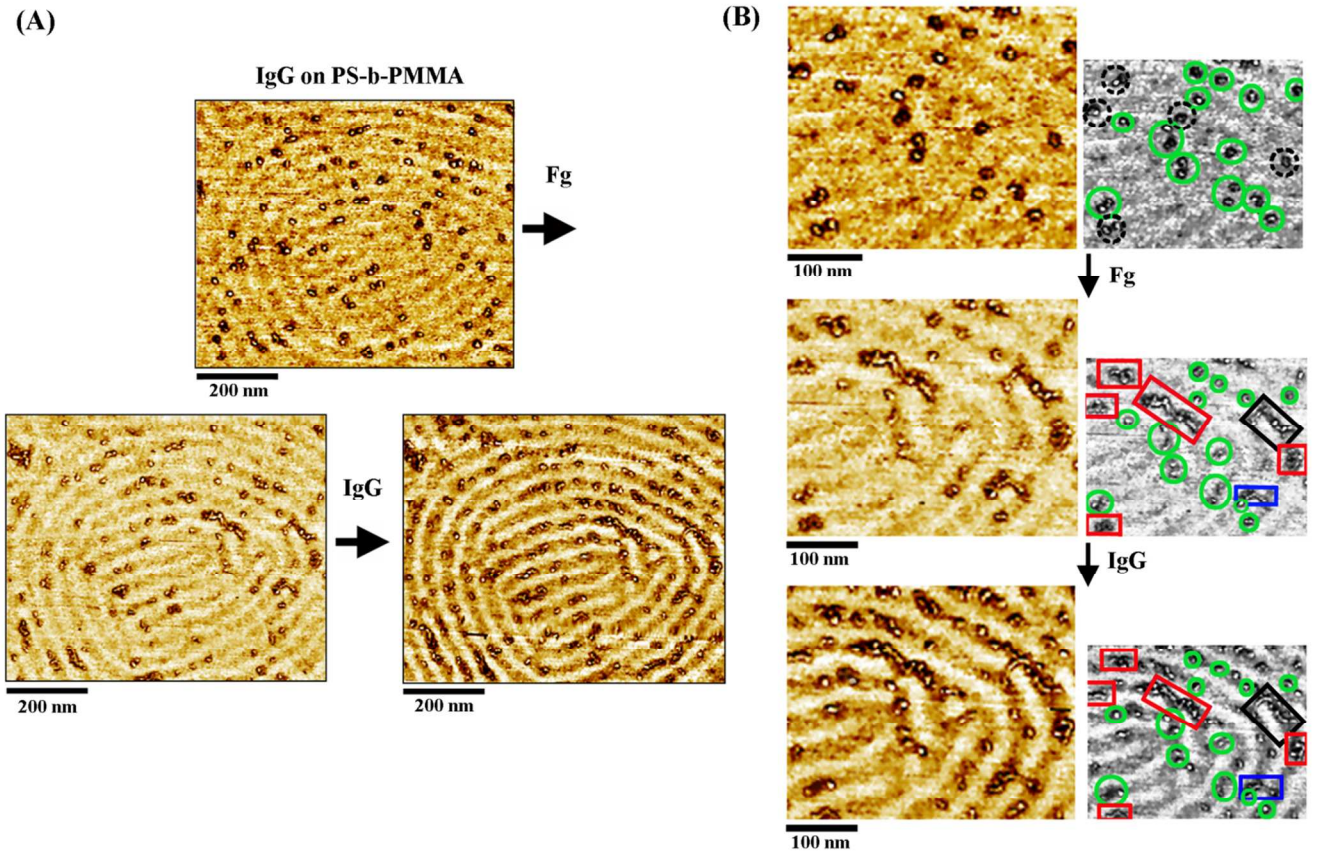

Figure 4. (A) Representative AFM images displaying the same PS-*b*-PMMA areas consecutively exposed to a protein solution of 0.1 μg/mL IgG for 30 s (1st stage), 1 μg/mL Fg for 15 min (2nd stage), and 0.1 μg/mL IgG for 5 min (3rd stage). **(B)** A zoomed-in area of (A) is shown as an example. The colored circles and boxes in the grey scale panels denote the different categories of protein adsorption pathways, as detailed in Fig. 3 using the same color code. From the sequence of AFM phase panels, it is evident that quite a few IgG molecules were exchanged with Fg molecules after the 2nd stage (red boxes). In contrast, no Fg molecules from the 2nd stage (red: exchange, blue: proximal adsorption,

black: distal adsorption) desorbed after the ensuing IgG deposition. When the 2nd and 3rd stage data were compared, all Fg molecules stayed bound. IgG molecules newly appearing on the surface after the 3rd stage adsorbed onto free surface sites, not taken up by IgG or Fg on the surface from the previous stages.

Dominant Protein Exchange Direction and Adsorption/Desorption Tendency. In hemostasis and thrombosis, bulk scale adsorption profiles of plasma proteins such as immunoglobulins and Fg have been extensively investigated.[5,37,53-55,59,61,72] In these studies, a protein exchange process that can occur on solid surfaces upon their exposure to different protein species under a competitive environment is known as the Vroman effect.[5,60,73] In brief, the Vroman process refers to the protein exchange phenomenon where early adsorbers (the more abundant, faster, and lower molecular weight species) are replaced by later arriving, larger species with higher surface affinity over time. However, the majority of the previous studies on Vroman exchange had to infer these molecular-level surface events indirectly from ensemble-averaged, spectroscopic or optical signals. This was due to the fact that the techniques, often used to study protein adsorption in the past, were more suited for interrogating collective protein behaviors. These methods relied on measuring the changes in resonance frequency,[31,36] surface plasmon resonance reflectivity,[43-45] IR absorption frequency,[30-32] fluorescence intensity,[39-42] and refractive index.[36-38] Yet, single protein behaviors can deviate significantly from the collective attributes of protein ensembles.[74-76]

Furthermore, the Vroman exchange process was reported to occur on some but not all surfaces. It was demonstrated that, for a ternary mixture of serum albumin (SA), IgG, and Fg, no exchange of the initially bound species of SA and IgG by Fg was seen on a hydrophobic surface of hexamethyldisiloxane, whereas the initially adsorbed species were completely replaced by Fg on the hydrophilic surfaces, such as positively charged diaminocyclohexane and negatively charged acrylic acid.[55,56] Hence, it is not yet entirely clear how the effect will scale down to competitive protein

adsorption cases occurring onto BCP nanodomain surfaces that inherently exhibit varying degrees of hydrophobicity/philicity. In these aspects, our results in Fig. 4 demonstrate that the protein exchange process of IgG by Fg indeed occurs on the PS-*b*-PMMA surface. More importantly, we provide direct experimental evidence at the single protein level that, regardless of the relative abundance of the two proteins, many events of Fg replacing IgG can take place on the BCP whereas no Fg molecules can be replaced by IgG. As further evidenced by the data presented in Fig. 5, such desorption/replacement of surface-bound IgG is triggered by the introduction of Fg, not by simply being exposed to a buffer solution. None of the initially bound IgG molecules left the BCP surface after the PBS treatment during the sequential introduction series shown in Fig. 5. We performed two additional control experiments on the BCP in which the 1st stage treatment involved 0.1 μg/mL IgG deposition for 30 s and the subsequent stage involved 15 min exposure to either PBS or deionized water (DI). In both controls, 99% of the IgG originally present on the BCP after the 1st stage remained on the surface after being exposed to PBS or DI. In comparison, it can be seen that some of those IgG molecules, which persisted on the BCP after the 2nd stage, were readily desorbed and replaced by Fg in the 3rd stage. An earlier study of Vroman effect assumed three different types of adsorbate population; rapidly exchangeable and desorbable macromolecules (type I population), a population of molecules subject to slow desorption but no replacement (type II), and totally irreversibly adsorbed molecules (type III).[77] It is likely that the IgG molecules in our experiment may presume the same three types of adsorbate populations on the nanoscale BCP surface. The exact attributes of IgG sub-populations making them more vulnerable to displacement by Fg rather than simple desorption are not entirely clear and an investigation is under way to determine the exact exchange mechanism.

For Fg, no cases of desorption were observed upon its initial adsorption to the BCP surface, regardless of the next treatment involving IgG or neat buffer. Hence, the AFM data in Figs. 4 and 5 reveal the dominant protein exchange direction and adsorption/desorption tendencies of IgG and Fg on PS-*b*-PMMA through direct visualization of the pertinent events at the individual protein level.

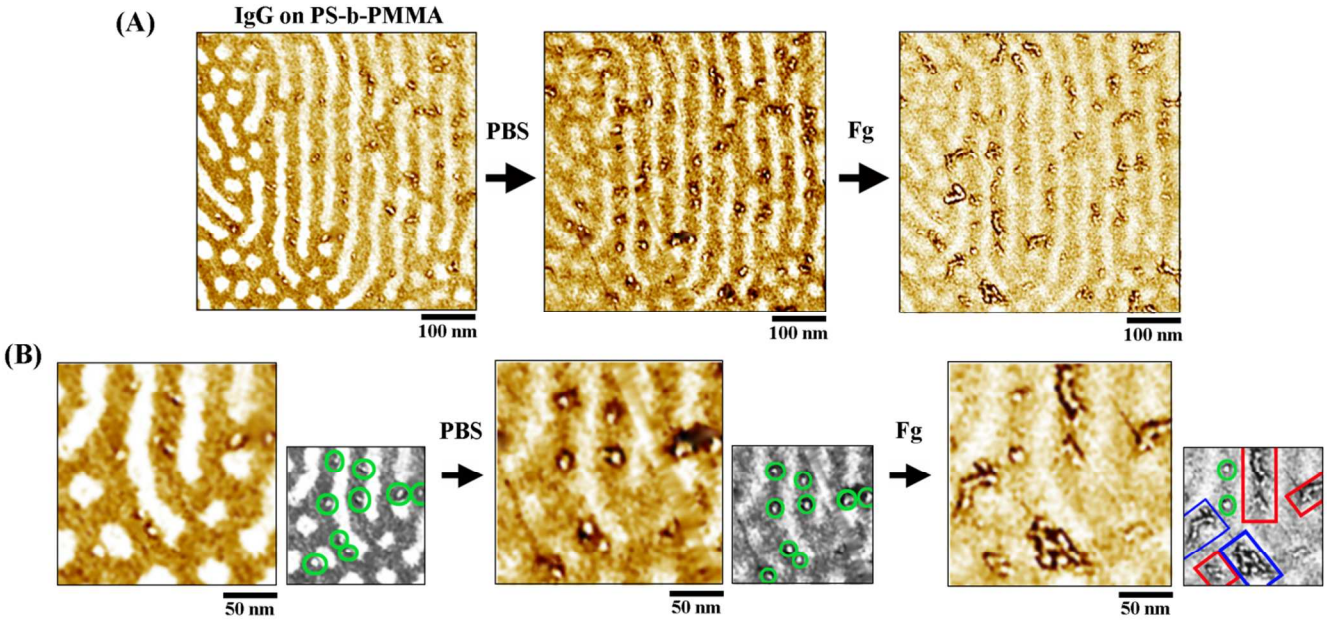

Figure 5. **(A)** The representative AFM phase scans display typical protein adsorption behaviors observed from the sequential exposure of a PS-*b*-PMMA surface to a solution containing 0.1 μg/mL IgG for 30 s (1st stage), PBS for 15 min (2nd stage), and 1 μg/mL Fg for 15 min (3rd stage). **(B)** To better guide the eye for tracking individual proteins between each stage, zoomed-in panels of the lower left quarter of the scans in (A) are provided as an example. The different categories of the protein adsorption pathways are marked for each protein using the same color code as Fig. 3. All IgG molecules adsorbed initially during the 1st stage remained bound on the surface after the 2nd stage of the neat buffer treatment. In contrast, the ensuing exposure of these surface-bound IgG molecules to Fg in the 3rd stage yielded many instances of IgG desorption and replacement.

Protein Mobility on Surface and Self-Association Degree. Surface diffusion of adsorbed proteins was found to be negligible in our system, occurring at a much slower timescale than that of the conformational rearrangement. In the case of Fg, no protein diffusion to other surface sites was observed in our data. This lack of diffusion may be due to the conformation that Fg takes upon

adsorption to the BCP surface. The 'lying-down' configuration may cause a high energetic penalty for Fg to undergo surface detachment/reattachment, greatly decreasing its mobility on the BCP surface. Similar to our observation, a bulk scale fluorescence study has also shown that there is no surface diffusion associated with Fg on both hydrophobic and hydrophilic surfaces.[78] For IgG, some instances of lateral translation were observed in our experiments. However, it should be noted that only a very small fraction (~ a few %) of IgG molecules moved on the BCP surface and their average travel distance was smaller than the diameter of the protein, placing them on the same PS nanodomain they were originally found on. The largest diffusion constant measured for IgG in our experiment was ~$5x10^{-15}$ cm^2/s. This value is comparable to the previously reported diffusion constant for another globular protein, lysozyme, with a reported value of $9x10^{-16}$ cm^2/s.[79] Thus, during a post-adsorption evolution, surface-induced conformational change plays a much more important role than 2D protein diffusion in our system.

We also noticed that the adsorption behaviors of IgG and Fg differed in that 'self-association' was frequently observed for Fg, but not for IgG. Self-association refers to protein adsorbing near its own kind. This is distinct from proximal adsorption events which points to the case of a protein adsorbing near a protein of another kind. The large self-association effect of Fg adsorption is evident in the AFM data presented in Figs. 1 and 2, in which the subsequent-stage Fg adsorption resulted in local regions of higher and lower Fg density due to self-association. This tendency was observed regardless of whether the BCP surface was initially populated with IgG or Fg. However, subsequent-stage IgG adsorption to the BCP surface containing either preadsorbed IgG or Fg molecules did not seem to induce the same level of self-association as Fg.

Pre-existing adsorption mechanisms such as clustering and tracking presume similar self-association processes of proteins on surfaces.[1,80,81] In the surface cluster model, each i-mer (monomer, dimer, trimer, etc.) attracts an incoming protein either directly next to the i-mer via a piggyback pathway or by diffusing towards a pre-existing cluster on the surface.[81] In comparison, the tracking model assumes that the approaching bulk proteins are attracted vertically but repelled in the lateral direction by

preadsorbed proteins. Thus, the sum of all electrostatic potentials is considered for the tracking and guiding of adsorbing proteins in the vicinity of preadsorbed proteins.[1,80] Based on our observation of extremely restricted lateral diffusion of Fg and a lack of local/global formation of vertically stacked, piggybacking Fg molecules, the tracking model seems to better explain the sequential adsorption events taking place in our system.

Influence of Preadsorbed Surface on Subsequent Stage Protein Adsorption. The presence of protein species on the surface from a prior stage may entirely change the adsorption behaviors of the subsequent stage protein species. In order to examine the potential effect of pristine versus preadsorbed PS-*b*-PMMA surfaces on subsequent stage protein adsorption, AFM data were collected from 5 independent samples subject to serial solution treatments. The single protein tracking data were then analyzed according to the different adsorption pathways as shown in Fig. 3. The analysis was carried out by tracking at least 15 different locations of 2 x 2 μm^2 in size per sample. The plots shown in Fig. 6 were subsequently obtained from the BCP samples that were first treated with IgG and then with Fg. The y-axis of the top to bottom graphs in Fig. 6(A), sharing the common x-axis as the number of preadsorbed IgG molecules, displays the total number of adsorbed Fg molecules, the number of Fg molecules adsorbed away from preadsorbed IgG, the number of Fg adsorbed adjacent to preadsorbed IgG, and the number of Fg molecules replacing IgG, respectively, all in units of counts per μm^2. A strong correlation was found between the number of newly adsorbed Fg molecules and the number of preadsorbed IgG proteins, see Fig. 6(A). In Fig. 6(B), the same four classes of Fg counts are charted on the y-axis, but this time using the bulk Fg solution concentration in $\mu g/mL$ as the common x-axis instead. Even for the same bulk Fg concentration, the number of newly adsorbed Fg molecules varied greatly on the different BCP surfaces containing varying IgG amounts. Henceforth, we will refer to this characteristic behavior where the amount of preadsorbed protein, rather than the bulk concentration of the newly arriving species, dictates the extent of protein adsorption in subsequent steps as preadsorbed surface-associated behavior.

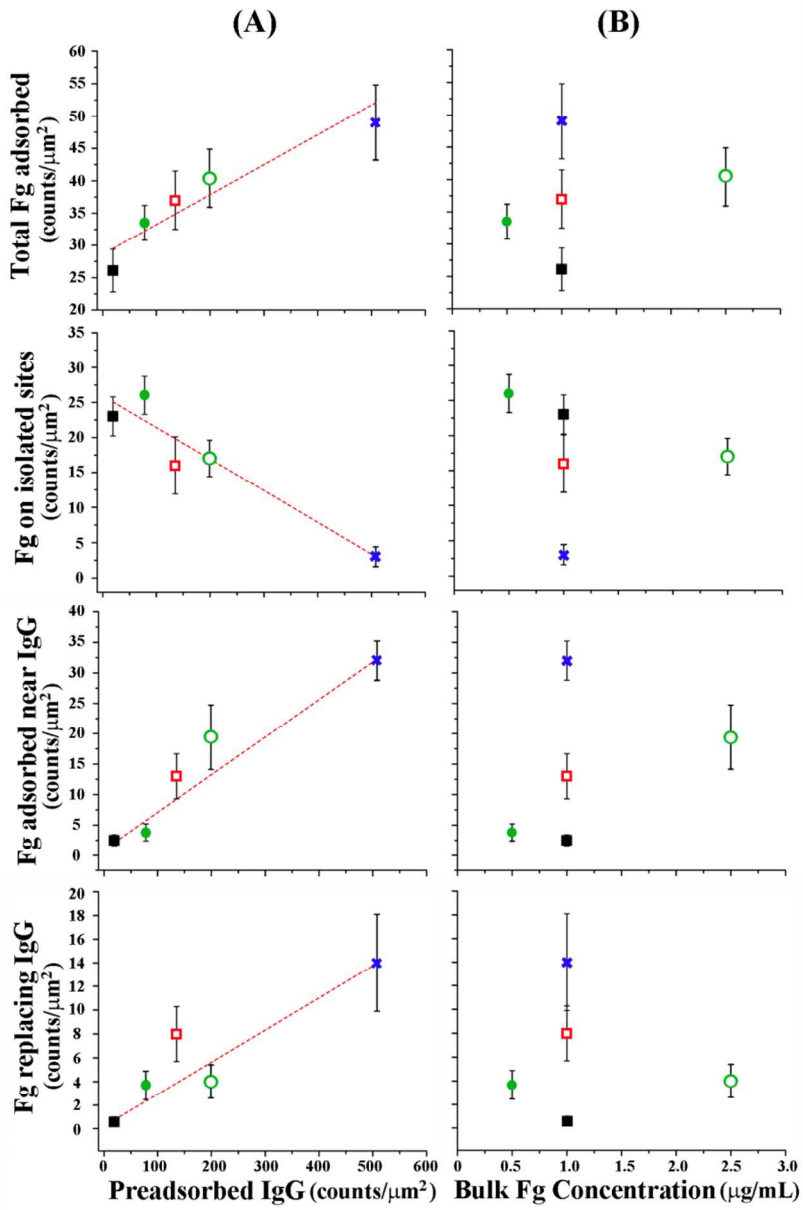

Figure 6. Preadsorbed surface-associated adsorption behavior identified from the sequential protein deposition experiment of IgG followed by Fg. **(A)** From top to bottom, the four graphs plot the number of preadsorbed IgG molecules versus the total number of adsorbed Fg, the number of distally adsorbed Fg, the number of proximally adsorbed Fg, and the number of Fg molecules replacing preadsorbed IgG, in units of counts (molecules) per μm^2. A highly linear correlation, either positive or negative depending on the adsorption pathway taken, was found between the adsorbed Fg molecules and the number of preadsorbed IgG proteins on PS-*b*-PMMA. As a guide to the eye, linear fits through the data

points are inserted along the data. **(B)** The same four classes of Fg counts are charted as a function of bulk Fg solution concentration in μg/mL. It can be seen that, even for the same bulk Fg concentration, the number of newly adsorbed Fg molecules varies greatly on different BCP samples containing varying amounts of preadsorbed IgG.

Fig. 7 further compares the distinctively different protein adsorption behaviors when they were introduced as an initial adsorber versus as a subsequent-stage adsorber containing preadsorbed proteins. We carried out control experiments where protein adsorption profiles were attained after depositing IgG or Fg onto a clean BCP surface. Fig. 7(A) displays adsorbed IgG amounts found on a clean PS-*b*-PMMA surface as a function of bulk IgG concentration, which is highly linear. Similarly, on a neat BCP template, a linear relationship was observed between the surface-adsorbed Fg counts and Fg solution concentration, as shown in Fig. 7(B). However, in the sequential deposition case of IgG → Fg, the amount of Fg adsorbed onto a BCP surface already containing IgG molecules showed strong dependence on the preadsorbed IgG molecules, rather than the bulk Fg concentration. In our sequential adsorption experiments, the concentrations of IgG and Fg were intentionally kept low, similar to the linear concentration regimes in Figs. 7(A) and 7(B). Yet, their sequential adsorption outcomes were different on a surface decorated with proteins. Such difference can be clearly seen by comparing the two plots displayed in Figs. 7(B) and 7(C) which were yielded by the deposition of the same protein, Fg, on a neat versus IgG-decorated BCP surface, respectively. The linearity with respect to the bulk solution concentration observed from Fg as the 1st adsorber species (Fig. 7(B)) was no longer present when it was introduced as a 2nd absorber (Fig. 7(C)). Data in Fig. 7(D) show that the Fg adsorption in the subsequent stage was largely influenced by the amounts of preadsorbed IgG on the BCP.

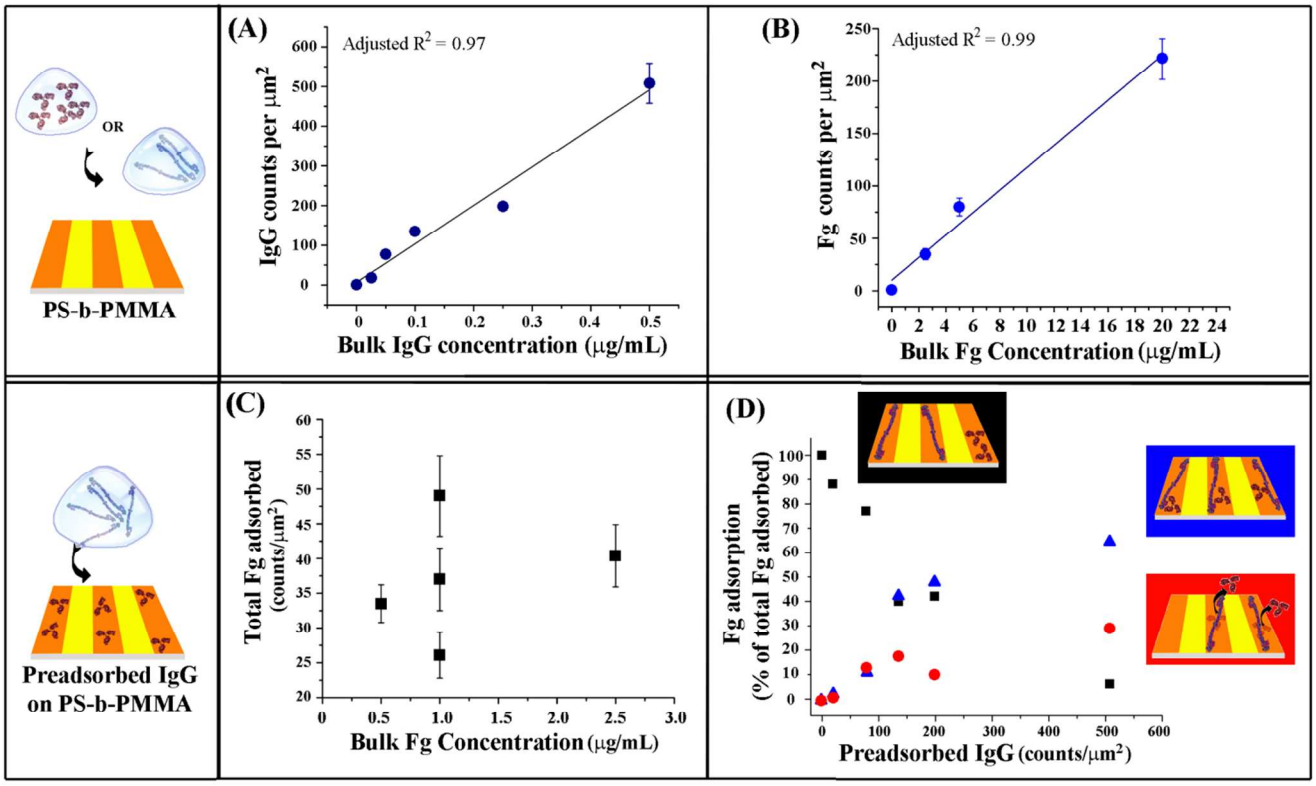

Figure 7. The characteristic protein adsorption behaviors found on neat versus pretreated PS-*b*-PMMA surfaces are summarized. **(A and B)** The control data were obtained by examining the case of (A) IgG and (B) Fg adsorption onto a clean BCP substrate with no preadsorbed proteins. (A) The plot of adsorbed IgG count versus bulk IgG solution concentration shows high linearity under the dilute concentration regime used. (B) The surface-adsorbed Fg counts also increase linearly with the bulk Fg solution concentration for the concentration range employed. **(C and D)** The data correspond to the preadsorbed surface-associated adsorption behavior of Fg when they were introduced as a subsequent stage adsorber to a BCP surface predecorated with IgG. (C) The plot displays the total adsorbed Fg counts versus Fg bulk concentration. (D) The occurrence frequencies of distal Fg adsorption, proximal Fg adsorption, and Fg replacing IgG are plotted. They are shown in black, blue, and red, respectively, in terms of its percent value with respect to the total Fg counts on the surface. Although the Fg solution concentrations used in the consecutive deposition experiments were well within the regimes yielding a highly linear correlation between the adsorbed amounts and the bulk concentration when deposited onto an untreated BCP surface as shown in (B), such a linear relationship was no longer present in the case of

the sequential Fg adsorption to IgG treated PS-*b*-PMMA. Fg adsorption in this case was dependent on preadsorbed IgG amounts on the surface, rather than its bulk concentration.

At pH 7.4, which we used for all our adsorption experiments, the two proteins and the PS-*b*-PMMA surface are charged negatively as they have isoelectric points (pIs) of 5.8-7.2 for IgG, 5.2 for Fg, 3.5-5 for PS, and 2-4 for PMMA.[69,72,82,83] From the point of view of electrostatic interaction, the PS-*b*-PMMA surface precovered with IgG molecules will present a more neutral or positively charged surface for the subsequent protein species to bind to, relative to the more negatively charged environment of a pristine BCP surface. This, in turn, may shift the energetic landscape of the surface such that the IgG-decorated BCP surface is more attractive to the next stage protein adsorption than the pristine BCP surface. Our experimental results in Figs. 6 and 7 seem to indicate that, even at a low density of preadsorbed IgG molecules of less than 500 molecules per μm^2 (surface coverage of less than 10%), the energetic landscape of the PS-*b*-PMMA surface can be altered enough to dominate the adsorption characteristics of the subsequent stage protein adsorbers. To test the hypothesis of the change in electrostatic landscape of the surface influencing subsequent protein adsorption, we conducted a simple control experiment involving a divalent cation of Mg^{2+} and the results are provided in Fig. S1[†] in the Electronic Supplementary Information section. When the net charge of a homopolymer PS surface became more positive than that of an untreated PS surface, the total number of the adsorbed Fg on the surface was increased by a 1.5 fold relative to the untreated case.

MC Simulations. We further substantiated the experimental outcomes for the different sequential adsorption cases with MC simulations of a simple model based on the energetic considerations of protein-protein repulsion and protein-surface attraction as detailed in the Methods section. The simulations were carried out for different 2D box scenarios,[62] an initially empty box (cases similar to Fig. 7(A and B)) versus a box with a certain amount of preadsorbed proteins (cases shown in Fig. 7(C and D)). IgG and Fg molecules were treated as small and large circular disks of 0.6σ and 1.2σ in size,

respectively. σ is a unit length associated with the arithmetic mean of the diameters of the two proteins. The specified sizes for the two disks modelling IgG and Fg in our simulations are similar to the values previously used for IgG and 'lying-down' Fg.[57] Per our experimental observations, proteins in the simulations were not allowed to move laterally once adsorbed on the surface and can only be desorbed. Subsequently, changes occurring in the 2D box such as the proximal, distal, and replacement adsorption events of the protein disks were examined.

Fig. 8(A) shows the adsorption simulation results by plotting the number of proteins per unit surface (counts/σ^2) as a function of the MC steps performed for the small proteins adsorbing/desorbing in an empty 2D box. After an initial increase, the counts/σ^2 value reaches a steady state count which does not change significantly despite new adsorption/desorption events occurring continuously over the whole duration of the simulation. The same trends were obtained from the simulation data in Fig. 8(B) which correspond to the large proteins adsorbing/desorbing to/from an empty substrate. From the outcomes of single adsorbers in a clean box as shown in Fig. 8, we determined the simulation conditions for bulk concentrations and MC steps that best reflect the experimental conditions, i.e. the low surface coverage and dilute bulk concentration regimes leading to the linear dependence in Figs. 7(A) and 7(B). We kept the unit energy-related parameter of $\frac{k_B T}{\varepsilon}$ as 10^{-3} where ε is the interaction strength that we used as the energy unit in the simulation, k_B is the Boltzmann constant, and T is the temperature. All simulation data and discussion in this paper correspond to this interaction energy regime.

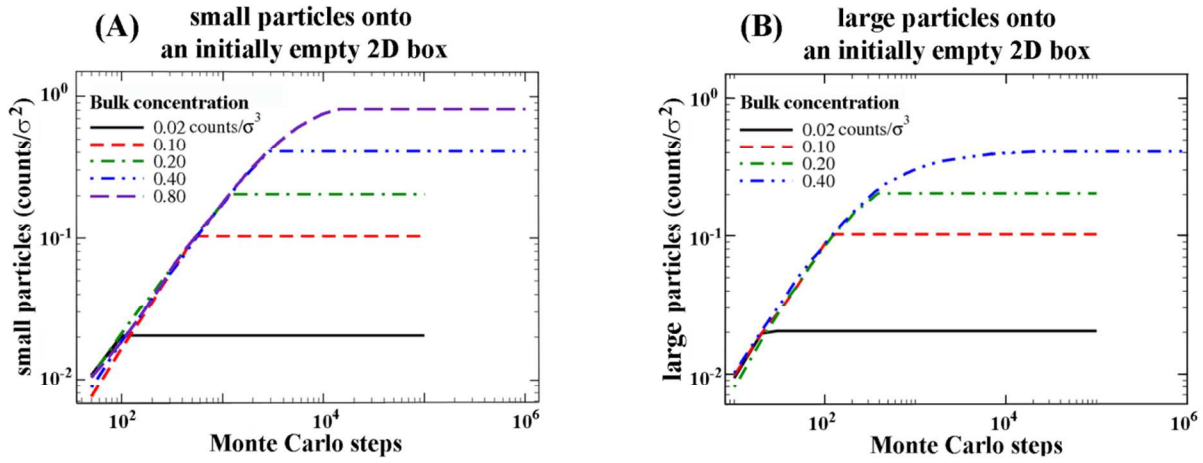

Figure 8. MC simulation results showing the bulk concentration-dependent adsorption behaviors monitored from single adsorbers added to an initially empty 2D box. The plots corresponding to different bulk concentrations display the number of **(A)** small and **(B)** large protein particles per unit surface adsorbed as a function of the MC steps.

Accordingly, we performed a set of MC simulations in which small proteins were preadsorbed onto the surface before introducing large proteins. The pre-bound small proteins on the surface can only be desorbed, whereas the large proteins in this simulation set can be adsorbed and desorbed. Illustrative snapshots of initial and final surface configurations from the simulations are provided in Fig. 9(A). By analyzing the location of newly appearing large proteins with respect to the locations of the preadsorbed small proteins, we identified various adsorption events resulting from the simulation considerations and further compared them with the experimental findings. Indeed, adsorption cases in which large proteins adsorb in areas with no small proteins nearby were seen in the simulation, consistent with the experimental observation of distal adsorption events. An example of such a case is indicated inside a black square in the right panel of Fig. 9(A). We also identified adsorption cases from the simulation corresponding to the experimentally observed proximal adsorption. An example of this case, in which large proteins adsorb in close proximity of preadsorbed small proteins, is enclosed within a blue square in Fig. 9(A). In addition, we found protein replacement events in the simulations, as marked with a red

square in Fig. 9(A). Agreeing with the experimental observations, adsorption of large proteins in these cases displaced one or more preadsorbed small proteins from the surface.

A statistical analysis of simulation results was subsequently performed on 50 independent initial samples. We compared the first and last configurations of each MC simulation and extracted the percentage of large proteins adsorbed on the substrate that belong to each case of proximal, distal, and replacement adsorption event. We considered that a large protein replaced one or more small proteins if at least one of the small proteins, located within a distance of 0.9σ from the adsorption loci in the initial configuration, was absent in the final configuration. If at least one small protein was present initially within the distance 1.5σ from the adsorption loci of a large protein and the large protein did not replace any small protein, we considered this to be a proximal adsorption case. Finally, we classified the adsorption of a large protein as distal if none of the above conditions were satisfied. As a result, the sum of all distinct cases is always equal to the total number of large proteins adsorbed on the surface. The data obtained are subsequently plotted in Fig. 9(B) as a function of the number of preadsorbed small proteins on the surface.

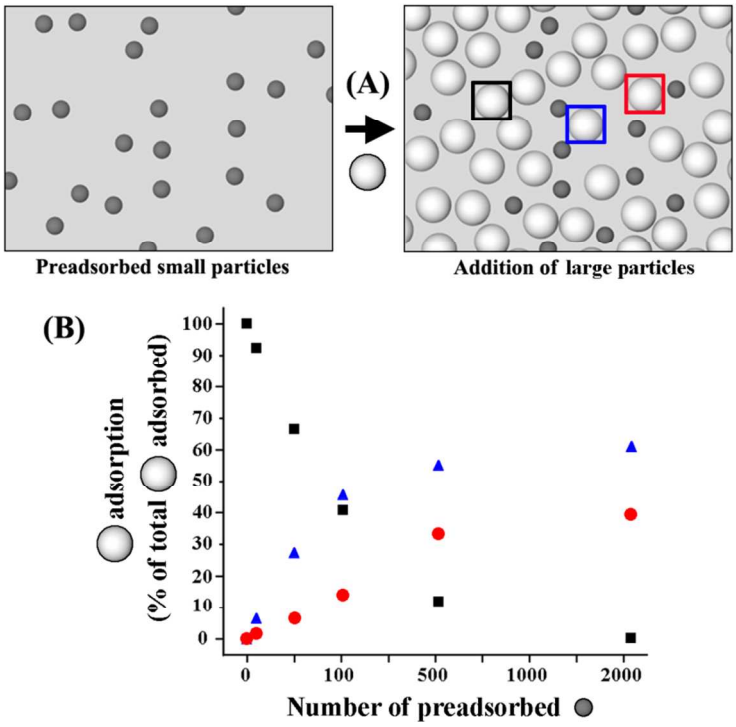

Figure 9. MC simulation outcomes showing adsorption of large proteins onto a 2D box preadsorbed with small proteins. **(A)** Snapshots from the simulations starting from preadsorbed small protein particles (left) and showing representative cases (right) of large particles being adsorbed. It can be clearly seen that the MC simulation can effectively reveal the experimentally observed cases of large particles adsorbing away from small particles (black square), close to preadsorbed small particles (blue), and by substituting a preadsorbed small particle (red). **(B)** Occurrence frequencies of the large particle adsorption events are plotted as a function of the number of preadsorbed small particles. The frequencies for the three different cases of large particle adsorption are displayed in percentages relative to the total number of large particle adsorbed.

When compared to the data obtained from direct AFM tracking of sequential adsorption events in Fig. 7, the MC simulation results in Fig. 9 show similar overall trends in the Fg adsorption frequency between the proximal, distal, and replacement adsorption events as a function of preadsorbed IgG particles. The good agreement between the experimental and simulation data suggests that the

simplified MC simulation considerations of protein-protein repulsion and protein-polymer surface attraction can be effectively used to estimate the general trend in the different pathways of sequential protein adsorption in a qualitative manner. Quantitative comparisons between the experimental and simulation outcomes will require additional and multilevel considerations, which is currently in progress. In this regard, the direct evidence of the dominant sequential protein adsorption tendencies and key characteristics found in our experiments may serve as useful guides. Specifically, additional simulational considerations such as the shape anisotropy difference between the two proteins, the varying self-association degree between proteins of the same kind, and the surface-induced conformational rearrangement may facilitate quantitative correlations to our experimental outcomes from competitive protein adsorption.

SUMMARY

We have revealed the major adsorption/desorption/replacement events and dominant pathways occurring in sequential protein adsorption onto a PS-*b*-PMMA surface and carried out MC simulations to further substantiate the experimental findings. AFM tracking of individual proteins adsorbed/desorbed on the same BCP surface locations between different treatments enabled us to unambiguously determine various adsorption-induced protein behaviors, such as the occurrence frequency associated with specific adsorption pathways, protein mobility on the surface, self-association tendency during adsorption, and directionality in protein exchange. We have also shown that the adsorption profiles of subsequent stage proteins onto a surface containing initial protein adsorbers differ significantly from those cases without pretreatment. As a result, we have provided direct experimental evidence at the single protein level that was not readily available in the past, especially for systems involving multiple proteins on nanoscale BCP surfaces. Such experimental proof may promote a new mechanistic understanding of competitive protein adsorption, validation of existing adsorption mechanisms, and design of new biomaterials and biosensors. Therefore, our endeavors will be

significant not only for advancing our fundamental knowledge on protein adsorption, but also for promoting technological applications of protein-polymer interfaces in the areas of biomaterials, biosensors/devices, and cell/tissue culture platforms.

ACKNOWLEDGEMENTS

The authors acknowledge financial support on this work by the National Science Foundation (Award No. CHE1404658) from the Macromolecular, Supramolecular and Nanochemistry Program under the Division of Chemistry.

Footnote

†Electronic supplementary information (ESI) available: AFM data of Fg adsorption on an untreated versus Mg^{2+}-modified homopolymer PS surface are provided in Fig. S1.

References

1. M. Rabe, D. Verdes and S. Seeger, *Adv. Colloid Interf. Sci.*, 2011, **162**, 87-106.
2. J. J. Gray, *Curr. Opin. Struct. Biol.*, 2004, **14**, 110-115.
3. K. Nakanishi, T. Sakiyama and K. Imamura, *J. Biosci. Bioeng.*, 2001, **91**, 233-244.
4. R. A. Latour, in *Encyclopedia of Biomaterials and Biomedical Engineering*, Informa Healthcare, 2nd edn., 2008, vol. 1, pp. 270-284.
5. L. Vroman and A. L. Adams, *J. Biomed. Mater. Res.*, 1969, **3**, 43-67.
6. V. Hlady and J. Buijs, *Curr. Opin. Biotechnol.*, 1996, **7**, 72-77.
7. A. Talapatra, R. Rouse and G. Hardiman, *Pharmacogenomics*, 2002, **3**, 1-10.
8. G. MacBeath and S. L. Schreiber, *Science*, 2000, **289**, 1760-1763.
9. M. F. Templin, D. Stoll, M. Schrenk, P. C. Traub, C. F. Vohringer and T. O. Joos, *Trends Biotechnol.*, 2002, **20**, 160-166.
10. Q. Xu and K. S. Lam, *J. Biomed. Biotechnol.* , 2003, **2003**, 257-266.
11. N. Kumar and J. Hahm, *Langmuir*, 2005, **21**, 6652-6655.
12. N. Kumar, O. Parajuli, A. Dorfman, D. Kipp and J. Hahm, *Langmuir*, 2007, **23**, 7416-7422.
13. N. Kumar, O. Parajuli, A. Gupta and J. Hahm, *Langmuir*, 2008, **24**, 2688-2694.
14. F. S. Bates and G. H. Fredrickson, *Annu. Rev. Phys. Chem.*, 1990, **41**, 525-557.
15. G. H. Fredrickson and F. S. Bates, *Annu. Rev. Mater. Sci.* , 1996, **26**, 501-550.
16. C. M. Bates, M. J. Maher, D. W. Janes, C. J. Ellison and C. G. Willson, *Macromolecules*, 2014, **47**, 2-12.
17. M. J. Maher, C. T. Rettner, C. M. Bates, G. Blachut, M. C. Carlson, W. J. Durand, C. J. Ellison, D. P. Sanders, J. Y. Cheng and C. G. Willson, *ACS Appl. Mater. Interf.*, 2015, **7**, 3323-3328.
18. J. Hahm, *Langmuir*, 2014, **30**, 9891-9904.
19. S. B. Darling, *Prog. Polym. Sci.*, 2007, **32**, 1152-1204.
20. B. Bhushan and S. R. Schricker, *J. Biomed. Mater. Res. A*, 2014, **102**, 2467-2480.
21. J. Malmström and J. Travas-Sejdic, *J. Appl. Poly. Sci.*, 2014, **131**, 40360.

22. S. Song, T. Xie, K. Ravensbergen and J.-i. Hahm, *Nanoscale*, 2016, **8**, 3496-3509.

23. S. Song, K. Ravensbergen, A. Alabanza, D. Soldin and J.-i. Hahm, *ACS Nano*, 2014, **8**, 5257-5269.

24. T. Xie, A. Vora, P. J. Mulcahey, S. E. Nanescu, M. Singh, D. S. Choi, J. K. Huang, C.-C. Liu, D. P. Sanders and J.-i. Hahm, *ACS Nano*, 2016, **10**, 7705-7720.

25. M. S. Lord, M. Foss and F. Besenbacher, *Nano Today*, 2010, **5**, 66-78.

26. J. Hahm, *J. Biomed. Nanotech.*, 2011, **7**, 731-742.

27. N. Kumar, O. Parajuli and J. Hahm, *J. Phys. Chem. B*, 2007, **111**, 4581-4587.

28. O. Parajuli, A. Gupta, N. Kumar and J. Hahm, *J. Phys. Chem. B* 2007, **111**, 14022-14027.

29. S. Song, M. Milchak, H. B. Zhou, T. Lee, M. Hanscom and J. I. Hahm, *Nanotech.*, 2013, **24**, 10.

30. M. Han, A. Sethuraman, R. S. Kane and G. Belfort, *Langmuir*, 2003, **19**, 9868-9872.

31. P. Roach, D. Farrar and C. C. Perry, *J. Am. Chem. Soc.*, 2005, **127**, 8168-8173.

32. P. Roach, D. Farrar and C. C. Perry, *J. Am. Chem. Soc.*, 2006, **128**, 3939-3945.

33. K. Cai, J. Bossert and K. D. Jandt, *Colloid. Surf. B: Biointerfaces*, 2006, **49**, 136-144.

34. F. A. Denis, P. Hanarp, D. S. Sutherland, J. Gold, C. Mustin, P. G. Rouxhet and Y. F. Dufrêne, *Langmuir*, 2002, **18**, 819-828.

35. R. Michel, S. Pasche, M. Textor and D. G. Castner, *Langmuir*, 2005, **21**, 12327-12332.

36. K. Rechendorff, M. B. Hovgaard, M. Foss, V. P. Zhdanov and F. Besenbacher, *Langmuir*, 2006, **22**, 10885-10888.

37. L. Vroman, A. L. Adams, G. C. Fischer and P. C. Munoz, *Blood*, 1980, **55**, 156-159.

38. P. Ying, Y. Yu, G. Jin and Z. Tao, *Colloid. Surf. B: Biointerfaces*, 2003, **32**, 1-10.

39. Y. L. Cheng, S. A. Darst and C. R. Robertson, *J. Colloid Interf. Sci.*, 1987, **118**, 212-223.

40. C. F. Wertz and M. M. Santore, *Langmuir*, 1999, **15**, 8884-8894.

41. C. F. Wertz and M. M. Santore, *Langmuir*, 2001, **17**, 3006-3016.

42. C. F. Wertz and M. M. Santore, *Langmuir*, 2002, **18**, 1190-1199.

43. Y. Arima and H. Iwata, *J. Mater. Chem.*, 2007, **17**, 4079-4087.

44. J. Breault-Turcot, P. Chaurand and J.-F. Masson, *Anal. Chem.*, 2014, **86**, 9612-9619.

45. R. J. Green, J. Davies, M. C. Davies, C. J. Roberts and S. J. B. Tendler, *Biomaterials*, 1997, **18**, 405-413.

46. C. Calonder, Y. Tie and P. R. Van Tassel, *Proc. Nat. Acad. Sci.*, 2001, **98**, 10664-10669.

47. V. Ball and J. J. Ramsden, *J. Phys. Chem. B*, 1997, **101**, 5465-5469.

48. Y. Tie, C. Calonder and P. R. Van Tassel, *J. Colloid Interf. Sci.*, 2003, **268** 1-11.

49. T. Pirzer, M. Geisler, T. Scheibel and T. Hugel, *Phys. Biol.*, 2009, **6**, 025004.

50. T. Pirzer and T. Hugel, *ChemPhysChem*, 2009, **10**, 2795-2799.

51. A. Toscano and M. M. Santore, *Langmuir*, 2006, **22**, 2588-2597.

52. T. F. Keller, J. Schönfelder, J. Reichert, N. Tuccitto, A. Licciardello, G. M. L. Messina, G. Marletta and K. D. Jandt, *ACS Nano*, 2011, **5**, 3120-3131.

53. S. Kidoaki and T. Matsuda, *Langmuir*, 1999, **15**, 7639-7646.

54. B. A. Cavic and M. Thompson, *Anal. Chem.*, 2000, **72**, 1523-1531.

55. B. Lassen and M. Malmsten, *J. Colloid Interf. Sci.*, 1997, **186**, 9-16.

56. B. Lassen and M. Malmsten, *J. Colloid Interf. Sci.*, 1996, **179**, 470-477.

57. P. Vilaseca, K. A. Dawson and G. Franzese, *Soft Matter*, 2013, **9**, 6978-6985.

58. C. H. Bamford, S. L. Cooper and T. Tsuruta, *The Vroman Effect*, VSP BV, The Netherlands, 1992.

59. S.-Y. Jung, S.-M. Lim, F. Albertorio, G. Kim, M. C. Gurau, R. D. Yang, M. A. Holden and P. S. Cremer, *J. Am. Chem. Soc.*, 2003, **125**, 12782-12786.

60. S. L. Hirsh, D. R. McKenzie, N. J. Nosworthy, J. A. Denman, O. U. Sezerman and M. M. M. Bilek, *Colloid. Surf. B: Biointerfaces*, 2013, **103**, 395-404.

61. A. Krishnan, C. A. Siedlecki and E. A. Vogler, *Langmuir*, 2004, **20**, 5071-5078.

62. D. Frenkel and B. Smit, *Understanding Molecular Simulations*, Academic Press San Diego, CA, 2nd edn., 2002.

63. K. Schwenke and E. D. Gado, *Faraday Discuss.*, 2015, **181**, 261-280.

64. R. J. Poljak, *Adv. Immunol.*, 1975, **21**, 1-33.

65. K. D. Elgert, *Immunology: Understanding The Immune System*, Wiley-Blackwell, Hoboken, NJ, 2nd edn., 2009.

66. C. E. Hall and H. S. Slayter, *J. Biophys. Biochem. Cytol.*, 1959, **5**, 11-27.

67. J. W. Weisel, G. N. Phillips and C. Cohen, *Nature*, 1981, **289**, 263-267.

68. J. W. Weisel, C. V. Stauffacher, E. Bullitt and C. Cohen, *Science*, 1985, **230**, 1388-1391.

69. R. R. Hantgan and S. T. Lord, in *Hemostasis and Thrombosis: Basic Principles and Clinical Practice*, eds. R. W. Colman, V. J. Marder, A. W. Clowes, J. N. George and S. Z. Goldhaber, Lippincott Williams & Wilkins, Philadelphia, PA, 2006, ch. 16.

70. Z. Yang, I. Mochalkin, L. Veerapandian, M. Riley and R. F. Doolittle, *Proc. Nat. Acad. Sci.*, 2000, **97**, 3907-3912.

71. J. Y. Joo, M. L. Amin, T. Rajangam and S. S. A. An, *Mol. Cell. Toxicol.*, 2015, **11**, 1-9.

72. T. Kawai, *Clinical Aspects of The Plasma Proteins*, Springer Verlag, Berlin, Germany, 2013.

73. T. A. Horbett and J. L. Brash, *Proteins at Interfaces II*, American Chemical Society, 1995.

74. R. Day and V. Daggett, *Proc. Natl. Acad. Sci. U.S.A.* , 2005, **102**, 13445-13450.

75. S. Y. McLoughlin, M. Kastantin, D. K. Schwartz and J. L. Kaar, *Proc. Natl. Acad. Sci. U.S.A.*, 2013, **110**, 19396-19401.

76. I. Tinoco and R. L. Gonzalez, *Genes Dev.*, 2011, **25**, 1205-1231.

77. A. Bentaleb, V. Ball, Y. Haïkel, J. C. Voegel and P. Schaaf, *Langmuir*, 1997, **13**, 729-735.

78. H. Nygren, S. Alaeddin, I. Lundström and K.-E. Magnusson, *Biophys. Chem.*, 1994, **49**, 263-272.

79. P. A. Mulheran, D. Pellenc, R. A. Bennett, R. J. Green and M. Sperrin, *Phys. Rev. Lett.*, 2008, **100**, 068102.

80. M. Rabe, D. Verdes, J. Zimmermann and S. Seeger, *J. Phys. Chem. B*, 2008, **112**, 13971-13980.

81. A. P. Minton, *Biophys. J.*, 2001, **80**, 1641-1648.

82. P. S. Bolt, J. W. Goodwin and R. H. Ottewill, *Langmuir*, 2005, **21**, 9911-9916.

83. J. K. Beattie, *Lab Chip*, 2006, **6**, 1409-1411.

TOC Graphics